J. Phys. D: Appl. Phys. **42** (2009) 165307 (9pp) doi:10.1088/0022-3727/42/16/165307

III-phosphides heterojunction solar cell interface properties from admittance spectroscopy

A S Gudovskikh[1,4], J P Kleider[2], R Chouffot[2], N A Kalyuzhnyy[3], S A Mintairov[3] and V M Lantratov[3]

[1] Saint-Petersburg Physics and Technology Centre for Research and Education of the Russian Academy of Sciences, Hlopina str. 8/3, 194021, St Petersburg, Russia
[2] LGEP; CNRS UMR 8507, SUPELEC, Univ Paris-Sud, UPMC Univ Paris 06, 11 rue Joliot-Curie, Plateau de Moulon, F-91192 Gif-sur-Yvette Cedex, France
[3] A.F. Ioffe Physico-technical Institute, Polytechnicheskaya str. 26, 194021 St Petersburg, Russia

E-mail: gudovskikh@edu.ioffe.ru

Received 26 March 2009, in final form 27 June 2009
Published 31 July 2009
Online at stacks.iop.org/JPhysD/42/165307

Abstract
GaInP solar cell interfaces were characterized by admittance spectroscopy. Admittance spectroscopy is shown to be sensitive to the band structure at the heterojunction interfaces. In particular, a correlation between activation energy of the capacitance step in a capacitance versus temperature plot and effective potential barrier for majority carriers is demonstrated, indicating a new method for the determination of potential barriers at heterointerfaces. Using this technique, the effective potential barrier for holes at the p-$Al_{0.53}In_{0.47}P$/p-GaAs interface is found to be equal to 0.6 eV. Effects of interface defects and spreading resistance in the emitter of solar cells are illustrated and discussed.

(Some figures in this article are in colour only in the electronic version)

1. Introduction

Heterostructures based on III-phosphides ternary alloys (GaInP, AlInP) have a wide field of applications in electronics, in particular, for the fabrication of solar cells. $Al_{0.53}In_{0.47}P/Ga_{0.52}In_{0.48}P$ heterojunctions are one of the most attractive candidates for the formation of the top subcell of multijunction GaInP/GaAs/Ge solar cells due to the matching of the lattice constant with the Ge substrate and due to the appropriate value of the band gap. The III-phosphides interfaces are very important issues in defining the properties of such heterojunction devices. A significant influence of the interface properties on GaInP solar cell performance was previously demonstrated in [1, 2]. Thus the study of the interface properties of these alloys is still required for further performance increase by optimization of the design and technology of the solar cells.

There is a wide range of techniques used for III–V interface characterization. The structural properties of the GaInP/GaAs interfaces were studied by XRD [3]. The values of the recombination velocity at the GaInP/GaAs interfaces were measured using time resolved photoluminescence [4]. A large number of techniques were used for the determination of such important interface parameters as values of the band offset: x-ray photoemission spectroscopy (GaInP/GaAs) [5], photoluminescence (PL) and PL excitation [6–10] and hydrostatic-pressure-dependent PL [11]. Also the values of the valence band offset (ΔE_V) and the interface charge density at the AlGaInP/GaAs interface were obtained by CV profiling [12]. The above-mentioned techniques rely on a given number of assumptions, which may limit their applications. For example, there is still an open question about band offset values because of a wide spread of these values obtained by different authors using those techniques for GaInP/GaAs (ΔE_V: 0.32–0.46 eV) and AlInP/GaInP (ΔE_V: 0.17–0.36 eV) interfaces [13].

[4] Author to whom any correspondence should be addressed.

In this paper we propose to use admittance spectroscopy in order to study the interface properties of III-phosphides solar cells. In general, capture and emission of charge carriers at and from interface states lead to charge changes and, therefore, may result in a capacitance contribution. This fact allows one to use admittance spectroscopy for defect characterization in space charge regions [14] and at heterointerfaces [15]. We will show here that admittance spectroscopy can also be used to deduce barrier heights at heterointerfaces, in particular, between the window layer and the emitter layer of III-phosphides solar cells.

2. Experiment and simulation details

Four different types of $Ga_{0.52}In_{0.48}P$ (hereafter, GaInP) solar cells were grown by MOVPE on p- and n-GaAs substrates including: p on n (p–n) structures without any window layer or with an additional p-$Al_{0.53}In_{0.47}P$ (hereafter, AlInP) or p-$Al_{0.8}Ga_{0.2}As$ (hereafter AlGaAs) window layer, as well as n on p (n–p) structures with an n-AlInP window layer. More details on the MOVPE fabrication procedure are given elsewhere [16]. The doping levels and thicknesses of the layers are given in table 1. AgMn : Ni : Au and AuGe : Ni : Au contacts to p-GaAs and n-GaAs, respectively, were used. Contact grid and ZnS/MgF_2 antireflection coating were formed on top of the $3.2 \times 8.3\,mm^2$ size solar cells. A heavy doped GaAs cap layer grown on top of the heterostructures for ohmic contact formation was etched in the photoactive area before antireflection coating deposition. The front contact grid consisted of 10 μm width and 2.8 mm length fingers with steps of 0.2 mm. The total area of the contact grid is about 8% of the solar cell area. In order to analyse the influence of the metal grid on capacitance measurements special mesa structures with full coverage of metal top contact of 0.9 mm diameter were also fabricated for p–n structures with a p-$Al_{0.53}In_{0.47}P$ window layer on the same wafer as for the solar cells. The solar cells and mesa structures design are schematically presented in figure 1.

The capacitance and conductance versus temperature and frequency measurements (C–T–ω and G–T–ω) were performed in a liquid nitrogen cryostat in a wide range of temperatures (90–350 K) and frequencies (20 Hz–1 MHz) using an HP4284A impedance meter.

In order to analyse the obtained results, computer simulations of the C–T–ω and G–T–ω curves were performed with the AFORS-HET 2.2 software [17]. We considered GaAs/window layer/GaInP/GaAs heterostructures, with ohmic front and back contacts (with electron and hole surface recombination velocities of $10^7\,cm\,s^{-1}$). The layers' parameters shown in table 1 were used in the calculations. The values of the band gap (E_g) and of the electron affinity (χ) used in the simulation are derived from the literature [13, 18–22] and presented in table 2. These values also determine those of the band offsets according to Anderson's approach [23]. The interface was described by introducing a very thin ($d = 1$ nm) defective GaInP layer between the emitter and the window layers. The energetic defect distribution (g_{it}) in this interface layer was taken as constant through the bandgap, assuming donor/acceptor-like defects in the lower/upper half of the bandgap. The interface defect density is described as $D_{it} = g_{it} \times d$. The electron and hole capture cross-sections were set at $10^{-14}\,cm^2$.

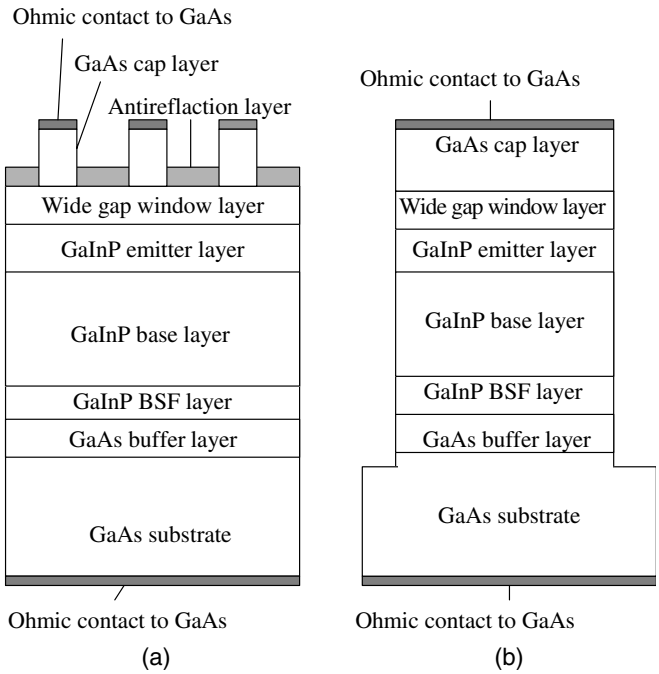

Figure 1. Schematic presentation of GaInP solar cells (a) and mesa structures (b) design.

3. Results

3.1. Simplified model

The calculated band diagrams at the top surfaces for different structures are presented in figure 2. The potential barriers for the majority carriers are formed at the interfaces due to band discontinuities. For instance, a high potential barrier for the holes is formed at the p-GaAs/p-AlInP interface due to the high valence band offset leading to the depletion of the whole p-AlInP window layer (figure 2(a)).

The simplest analysis of the admittance spectra may be made in terms of the equivalent circuit, as described in figure 3. C_W and G_W are the capacitance and conductance of the depletion region of the p–n junction in GaInP. These are in series with C_b and G_b, being the parallel capacitance and conductance of the depletion region formed by the potential barriers at the 'cap GaAs/window' and 'window/GaInP emitter' interfaces (or 'cap GaAs/GaInP emitter' interface in the case of the structure without a window layer).

Neglecting the conductance of the p–n junction G_W, the equivalent parallel capacitance, C_p, and conductance, G_p, are equal to

$$C_p = \frac{C_W \cdot G_b^2 + \omega^2 \cdot C_W \cdot C_b \cdot (C_W + C_b)}{G_b^2 + \omega^2 \cdot (C_W + C_b)^2}, \tag{3.1}$$

$$G_p = \frac{\omega^2 \cdot C_W \cdot G_b}{G_b^2 + \omega^2 \cdot (C_W + C_b)^2}, \tag{3.2}$$

Table 1. Values of the doping level/thickness (cm^{-3})/(nm) of the layers for the four types of structures.

Layer	n–p (AlInP)	p–n (AlInP)	p–n (no window)	p–n (AlGaAs)
GaAs cap	$2 \times 10^{18}/300$	$10^{19}/300$	$10^{19}/300$	$10^{19}/300$
Window	$Al_{0.53}In_{0.47}P$	$Al_{0.53}In_{0.47}P$	No	$Al_{0.8}Ga_{0.2}As$
	$2 \times 10^{18}/30$	$2 \times 10^{17}/30$	—	$2 \times 10^{17}/30$
GaInP emitter	$10^{18}/50$	$5 \times 10^{17}/50$ i/100	$5 \times 10^{17}/50$ i/100	$5 \times 10^{17}/50$ i/100
GaInP base	$10^{17}/800$	$10^{17}/920$	$10^{17}/920$	$10^{17}/920$
GaInP BSF	$2 \times 10^{18}/50$	$2 \times 10^{18}/50$	$2 \times 10^{18}/50$	$2 \times 10^{18}/50$
GaAs buffer	$2 \times 10^{18}/150$	$2 \times 10^{18}/150$	$2 \times 10^{18}/150$	$2 \times 10^{18}/150$

Table 2. Values of the band gap (E_g), electron affinity (χ) of the layers as well as band gap offsets (ΔE_C, ΔE_V) of different interfaces used in the simulations are presented.

Material	E_g (eV)	χ (eV)	Interface	ΔE_C (eV)	ΔE_V (eV)
GaAs	1.42 [18]	4.07 [18]	GaAs/GaInP	0.06	0.375
$Ga_{0.52}In_{0.48}P$	1.85 [19]	4.01 [21]	GaAs/AlInP	0.3	0.63
$Al_{0.53}In_{0.47}P$	2.35 [20]	3.78 [21]	GaInP/AlInP	0.23	0.27
$Al_{0.8}Ga_{0.2}As$	2.09 [13]	3.53 [22]	GaAs/AlGaAs	0.54	0.13
			GaInP/AlGaAs	0.48	0.24

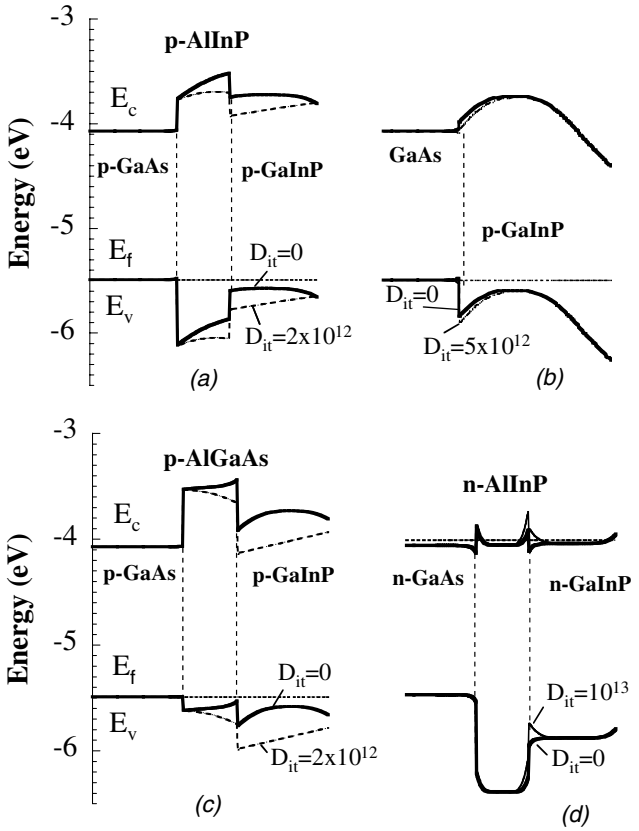

Figure 2. Band diagrams at the front surface calculated with different values of D_{it} (in eV^{-1} cm^{-2}) for the four types of structures: p–n structure with p-AlInP window layer (*a*), without window layer (*b*), p-AlGaAs window layer (*c*) and n–p structure with n-AlInP window layer (*d*).

where ω is the angular frequency. Assuming that G_b is dominated by thermoionic emission over the potential barrier it may be expressed as

$$G_b = G_0 \cdot \exp\left(-\frac{q \cdot \varphi_b}{k \cdot T}\right), \tag{3.3}$$

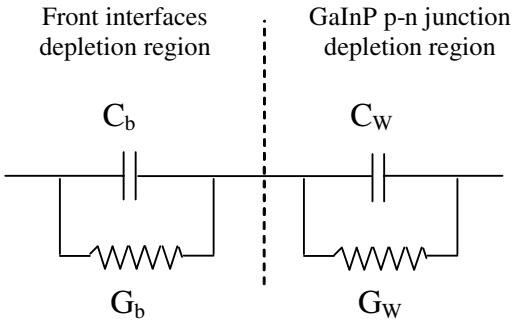

Figure 3. Simplified equivalent circuit for the admittance.

where G_0 is the temperature dependent thermoionic emission pre-factor, q is the electron charge, φ_b is the effective height of the potential barrier, k is Boltzmann's constant and T is the temperature.

The calculated temperature dependences of C_p and G_p/ω, using formulae (3.1), (3.2) and (3.3) with temperature independent values of C_W, C_b and G_0 for different frequencies are presented in figure 4. Capacitance curves exhibit a step. At low temperatures (high frequencies) the transport of the majority carriers through potential barriers at the interfaces is limited, i.e. the conductance G_b is low and the total capacitance can be expressed as C_W in series with C_b. At higher temperatures (lower frequencies) the majority carriers can overpass the potential barriers at the interfaces, i.e. conductance G_b is large enough to shunt the capacitance C_b and the total capacitance is equal to the capacitance of the depletion region of the p–n junction, C_W.

The step in the capacitance curves is accompanied by a maximum in conductance. The conductance maximum in the $G_p/\omega(T)$ curves corresponds to the inflection point in the $C_p(T)$ curves as demonstrated in figure 4(*b*), where the derivative of the capacitance against temperature, dC_p/dT, is presented. The position of this feature is shifted to higher temperature when increasing the frequency. This shift in the temperature position versus frequency may be used

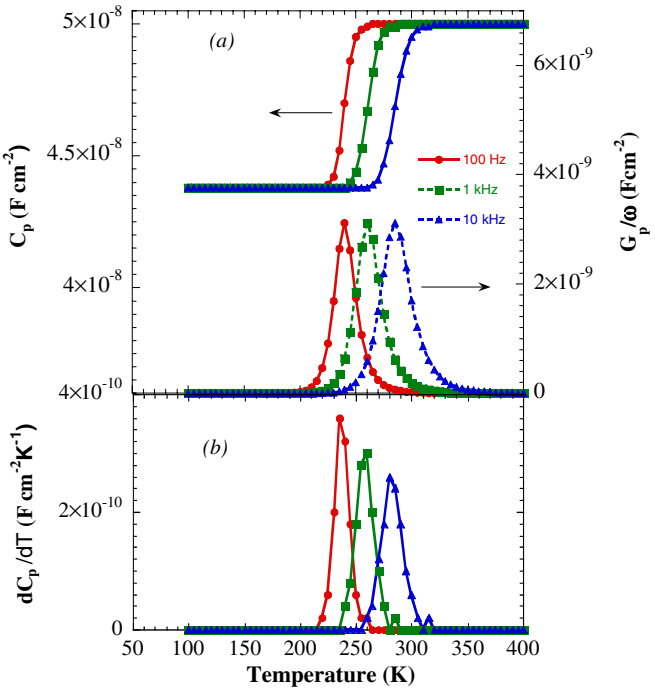

Figure 4. Calculated curves of C_p and G_p/ω versus temperature for 100 Hz, 1 kHz and 10 kHz using $C_W = 5 \times 10^{-8}$ F cm^{-2}, $C_b = 3.5 \times 10^{-7}$ F cm^{-2}, $G_0 = 10^9$ Ohm^{-1} cm^{-2} and $\varphi_b = 0.6$ eV (a). Calculated dC_p/dT and G_p/ω curves (b).

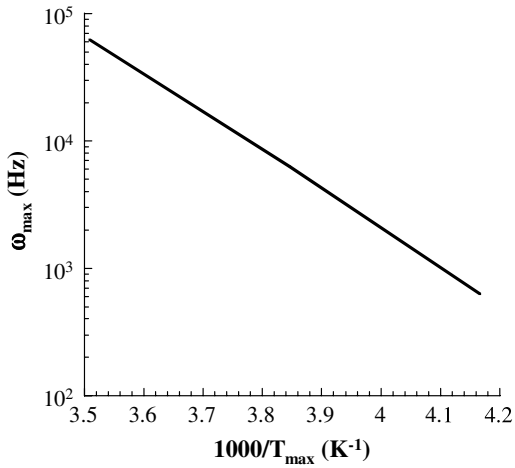

Figure 5. An Arrhenius plot of the frequency dependence obtained from the maximum in G_p/ω versus T or inflection point in dC_p/dT versus T curves.

to obtain the activation energy of the underlying process. An Arrhenius plot of the measurement frequency at the conductance maximum (or at the inflection point in the capacitance), shown in figure 5, gives an activation energy equal to the potential barrier height φ_b (0.6 eV) used in the calculations.

It is worth stressing that, while a step in C–T–ω (peak in G/ω–T–ω) is usually attributed to the response of defects to the ac modulation [14], these features are observed in our calculated admittance curves although no defects were introduced in these calculations, and they are

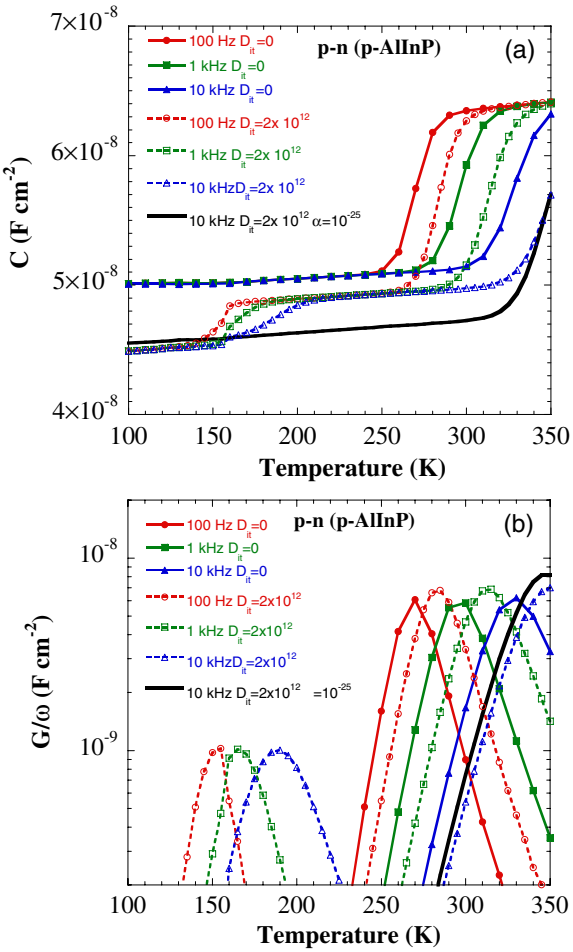

Figure 6. Simulated C–T–ω (a) and G/ω–T–ω (b) curves for the p–n structure with p-AlInP window in three cases: no interface states (full symbols and plain lines), $D_{it} = 2 \times 10^{12}$ eV^{-1} cm^{-2} and $\sigma = 10^{-14}$ cm^2 (open symbols and dashed lines), $D_{it} = 2 \times 10^{12}$ eV^{-1} cm^{-2} and $\sigma = 10^{-25}$ cm^2 (solid line).

due here to the activation of transport across a potential barrier. This simplified model demonstrates the way to directly determine the effective potential barrier height using admittance spectroscopy. Obviously, the determination of the barrier height from experimental data will be affected by the temperature dependence of parameters such as the thermoionic emission pre-factor G_0. However, these temperature dependences are weak compared with the activated barrier overcoming, and the related error in the determination of the potential barrier if one just neglects these temperature variations is of the order of a few meV.

3.2. Simulation results

For a more detailed analysis numerical simulations of the admittance spectra were performed for the four different structures. In these simulations, the parameters specific to each layer (given in tables 1 and 2) were taken into account.

First, the simulation of C–T–ω and G/ω–T–ω curves was performed for the structures without interface defects ($D_{it} = 0$). An example of the calculated C–T–ω and G/ω–T–ω curves for the p–n structure with the p-AlInP

window layer at zero bias is presented in figure 6. C–T–ω curves have a step in capacitance at 250–350 K, which is accompanied by a peak in G/ω–T–ω curves. The activation energy obtained from an Arrhenius plot of the measurement frequency at the conductance maximum (also corresponding to the inflection point in the capacitance) is equal to 0.6 eV. The value of the activation energy of the capacitance step corresponds to the difference between the valence band edge (E_v) and the Fermi level (E_F) at the p-GaAs/p-AlInP interface (figure 2(a)). Taking into account that the top GaAs cap layer is degenerated, the activation energy of the simulated curves corresponds to the valence band offset (ΔE_V) at the 'cap GaAs/window layer' interface.

Similar features in the admittance were observed in the calculated C–T–ω curves of the other structures, as can be shown in figure 7. The p–n structure without a window layer (figure 7(a)) has a step at low temperature (120–170 K) and an activation energy of 0.34 eV. The p–n structure with the p-AlGaAs window layer (figure 7(b)) has a step at lower temperature (80–120 K) with a lower activation energy of 0.2 eV. The n–p structure with n-AlInP window layer (figure 7(c)) has a double step at lower temperature (60–100 K) with activation energies of about 0.13 and 0.2 eV. The obtained values of the activation energy are equal to the potential barrier heights for the majority carriers at the corresponding front interfaces.

We should note that for the n–p structure with n-AlInP window layer the p-GaInP back surface field (BSF) layer is highly doped (about 2×10^{18} cm^{-3}). Tunnelling through the potential barrier (spike of the valence band) at the back p-GaInP/p-GaAs interface is then assumed to be the dominant process in the hole transport. Therefore, this back interface was not taken into account in the simulations where the tunnelling effect is not implemented.

In a second set of simulations, the defect density, D_{it}, was introduced at the 'window/emitter' interface ('cap layer/emitter' interface in the case of no window layer). For the p–n structure with p-AlInP window layer the presence of the interface states with $D_{it} = 2 \times 10^{12}$ eV^{-1} cm^{-2} leads to the appearance of a second step in the capacitance at low temperature $T < 120$ K (figure 6). This second step is due to the capture and emission processes at/from the interface states. This is clearly demonstrated from the simulation. Indeed, when negligible capture cross-section values ($\sigma = 10^{-25}$ cm^2) were introduced, no second step was observed. For other p–n structures the presence of interface states at p-GaAs/p-GaInP and p-AlGaAs/p-GaInP front interface leads to a shift of the capacitance step position (figures 7(a) and (b)) along the temperature axis. The shift is slight for D_{it} up to 10^{12} eV^{-1} cm^{-2} and it increases with increasing D_{it}. This is due to changes in band bending at the interface due to the pinning effect of the Fermi level and therefore the height of the potential barrier for majority carriers, as can be seen in the band diagram calculated with corresponding values of D_{it} (figures 2(b) and (c)).

For n–p structures with n-AlInP window and D_{it} at n-AlInP/n-GaInP front interface up to 10^{12} eV^{-1} cm^{-2} no changes in the C–T–ω curves are observed (figure 7(c)), while

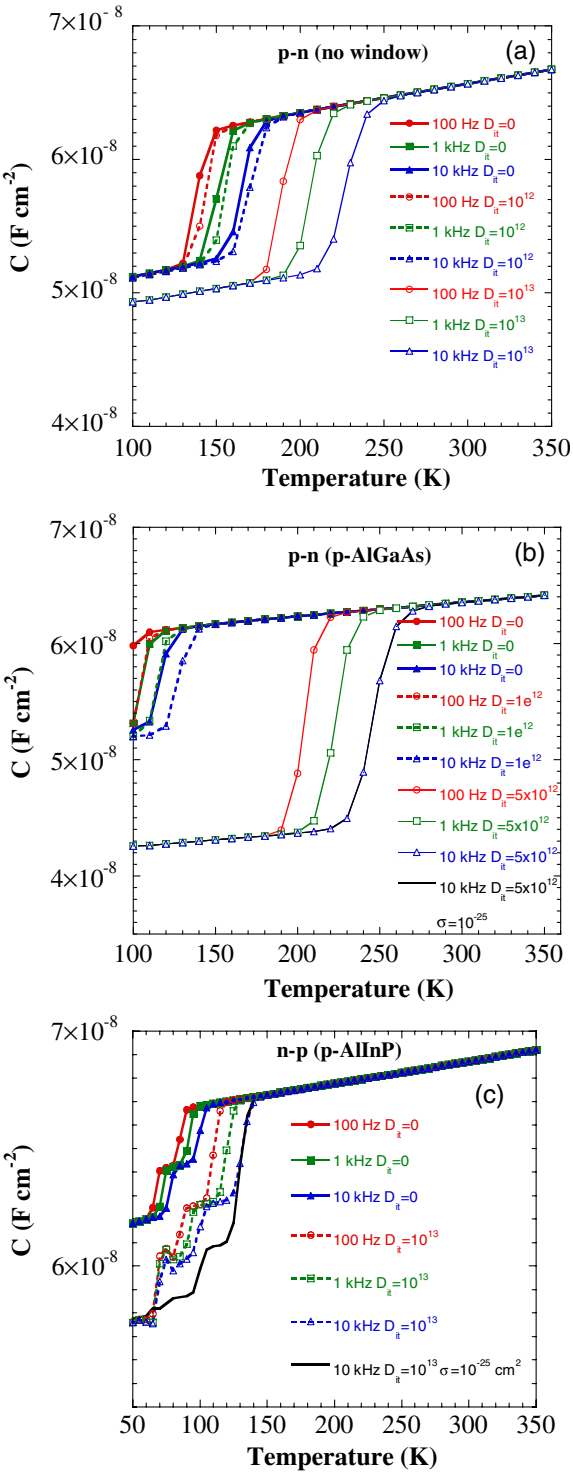

Figure 7. Simulated C–T–ω curves for the p–n structure without (a) and with (b) p-AlGaAs window layer and also for the n–p structure with n-AlInP window layer (c) with various densities of interface states D_{it} (in eV^{-1} cm^{-2}).

increasing D_{it} to 10^{13} eV^{-1} cm^{-2} leads to a shift of the step in capacitance, which is related to transport phenomena at the front interface, towards higher temperature (120–180 K) and to an increase in the step amplitude. This occurs because band bending (caused by pinning effect) at the front interface leads

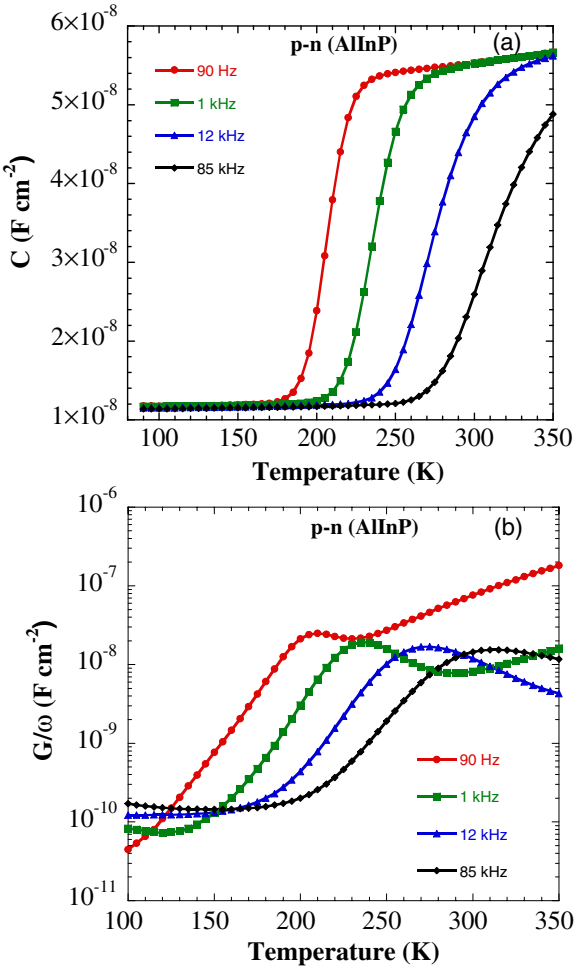

Figure 8. Experimental C–T–ω (a) and G/ω–T–ω (b) curves for the p–n structure with p-AlInP window measured at 0 bias.

to an increase in the potential barrier for electrons at the front n-AlInP/n-GaInP interface (figure 2(d)). Another step, which can be observed in the lower temperature range ($T < 120$ K) appears. It is caused by capture and emission processes at the interface states. This step is not observed when negligible capture cross-section values ($\sigma = 10^{-25}$ cm^2) are introduced (figure 7(c)).

We should stress that the behaviour of simulated C–T–ω curves, which is caused by band bending due to the Fermi level pinning effect is strongly dependent on the distribution of the interface states density.

3.3. Experimental results

The measured C–T–ω and G/ω–T–ω curves at zero applied dc voltage for the p–n structure with p-AlInP window are presented in figure 8. The values of the capacitance and conductance are divided by the whole area of the solar cells. C–T–ω curves exhibit a well-pronounced step at 200–300 K, which is accompanied by a maximum in G/ω–T–ω in the curves. The activation energy obtained from an Arrhenius plot of the measurement frequency at the conductance maximum is about 0.38 eV. Examples of the measured C–T–ω curves at

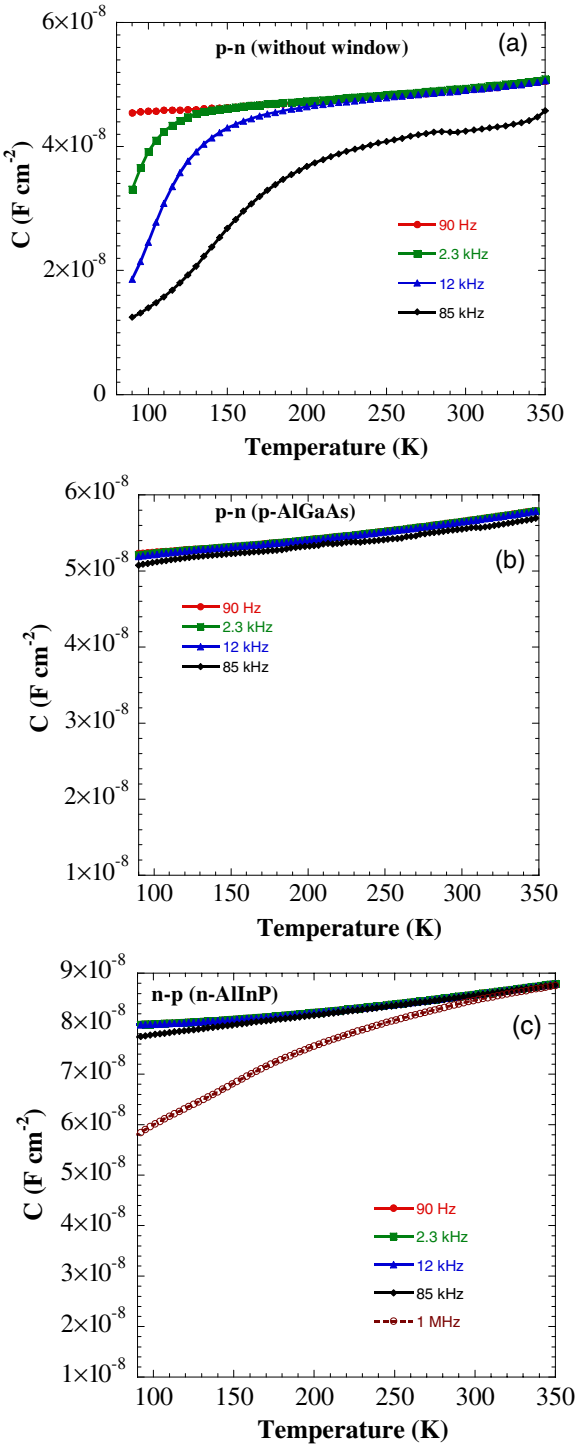

Figure 9. Experimental C–T–ω curves for the p–n structure without (a) and with p-AlGaAs (b) window layer and for the n–p structure with n-AlInP window layer (c) measured at 0 V bias.

zero applied dc voltage for the other structures are presented in figure 9. The p–n structure without a window layer (figure 9(a)) has a step at lower temperatures (100–150 K) and a lower activation energy of about 0.05–0.06 eV. For the p–n structure with the AlGaAs window layer (figure 9(b)) no step has been observed and for the n–p structure with the n-AlInP window layer (figure 9(c)) the step is supposed to appear at a lower temperature.

4. Discussion

The results of the numerical simulations without interface states are in good agreement with the model based on the simplified equivalent circuit. The C–T–ω curves exhibit a step accompanied by a peak in the G/ω–T–ω curves with activation energy equal to the effective barrier height.

According to the simulations, a high density of interface states may lead to the appearance of a second step (peak) in capacitance (conductance), which can be used as a rough estimate of the interface quality. More importantly, interface states even at lower densities also affect the band structure at the interface leading to changes in the effective barrier height. The actual values of the effective barrier heights, being a very important issue for the design and analysis of the solar cell structures, can thus be determined by admittance measurements. In other words, interface states may not be responsible for a direct signature in admittance measurements through a step in the C–T–ω curves and a peak in the G/ω-T-ω curves (due to trapping and detrapping of carriers). However, such step/peak features observed in the admittance measurements can originate from the onset of transport across energy barriers that depend on the band bending which is influenced by interface states.

Qualitative correlation between experiment and simulation was obtained. Both experiments and simulations demonstrate that: p–n structures with p-AlInP window exhibit a step in capacitance at higher temperatures with higher activation energy; p–n structures without window exhibit a step at lower temperatures with a lower value of activation energy; for p–n structures with the p-AlGaAs window and for n–p structures with the n-AlInP window the step is supposed to be located out of the range of experimental temperatures and frequencies.

However, a significant difference between experiment and simulations in the absolute value of the capacitance below the step and in the value of the activation energy is observed. This difference may be explained in terms of the geometry of the top metal electrode grid, which cannot be taken into account in a 1D simulation. At high temperatures the effective area of the junctions is equal to the whole structure area, while at low temperatures the lateral conductance of the emitter becomes smaller and the effective area of the capacitance C_W reduces to the area of the metal grid, leading to a significant decrease in the capacitance. This is illustrated by the capacitance versus bias measurements performed at 300 and 100 K on p–n solar cells with the p-window layer shown in figure 10. The capacitance at 100 K is much smaller than at 300 K and the corresponding slope of the inverse squared capacitance is larger. At 300 K this slope corresponds to the doping levels of the structure if one considers that the effective area determining the capacitance corresponds to the whole cell area. We should note that according to the low values of the ionization energy of Si donors in GaInP [24] the concentration of ionized donors should not be changed from 300 to 100 K and therefore no changes in the slope should occur if the effective area of the measured capacitance was unchanged. In contrast, a decrease (here by a factor of 3) of this effective area could explain the observed increase in the slope.

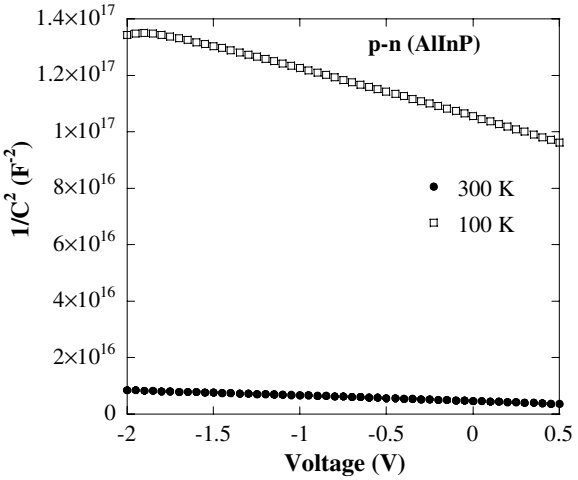

Figure 10. Experimental $1/C^2$ versus applied bias curves for the p–n structure with p-AlInP window, measured at 1 kHz and at 300 and 100 K.

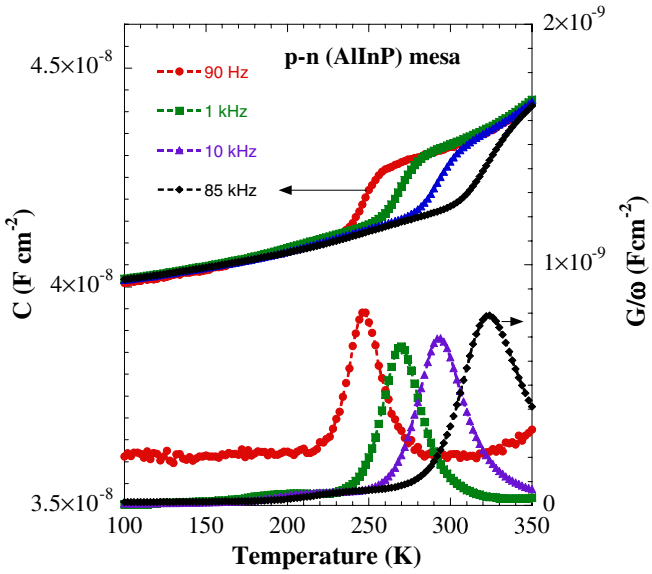

Figure 11. Experimental C–T–ω curves for the p–n mesa structure with p-AlInP window, measured at 0 V.

In order to check the influence of the contact grid on the admittance measurements a test mesa structure was fabricated. The admittance measurements performed on the p–n mesa structures with the p-AlInP window (fabricated on the same type of wafer as the solar cells) are presented in figure 11. The amplitude of the capacitance step in the C–T–ω curves is significantly smaller compared with that of the solar cells being in agreement with simulations results.

Another important issue can be deduced from the measurements performed on the mesa structures. Indeed, the activation energy of the capacitance step in the C–T–ω curves being about 0.6 eV, this corresponds to the value obtained from the simulations and it is in good agreement with the values of ΔE_V at the GaAs/AlInP interface reported by other authors, 0.54–0.63 eV [12, 25]. The obtained value of E_a corresponds also to that of the effective barrier for the holes used in analysis of the I–V curves under illumination [2]. We should stress that

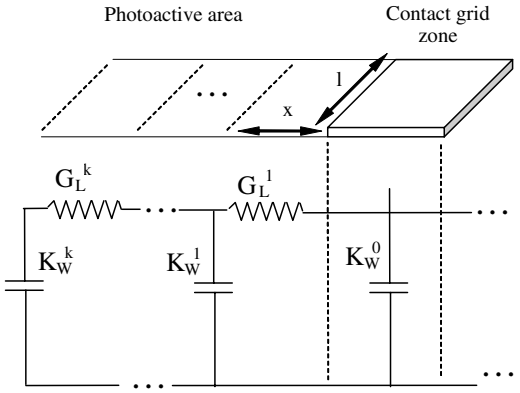

Figure 12. Simplified equivalent circuit of the p–n junction depletion region capacitance taking into account the spreading in p-GaInP emitter.

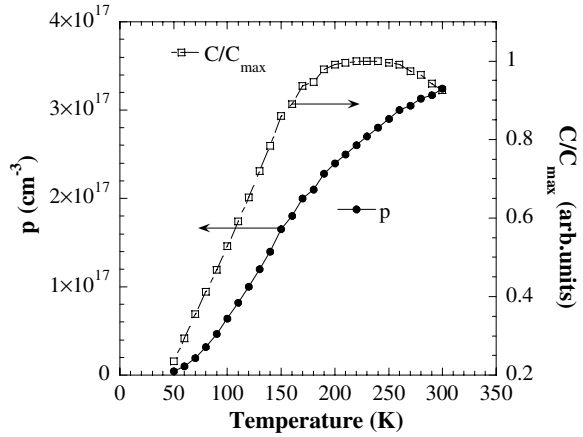

Figure 13. Calculated temperature dependence of the hole concentration in p-GaInP emitter layer and calculated for 100 Hz normalized equivalent capacitance of the circuit presented in figure 12.

the correlation between the activation energy of the C–T–ω curves and the value of the effective potential barrier is a very important issue, which can be used for the characterization of different isotype heterojunctions.

The lower values of E_a by 30–40% for solar cells compared with mesa structures may also be explained by the geometry of the contact grid, which leads to the spreading and therefore changing in the active area of the top contact. A further study using 2D modelling should be performed to explain the difference in E_a for solar cells and mesa structures. The observed difference between solar cells and mesa structures demonstrates that 1D simulation results should be compared with experimental results obtained on mesa structures only.

The influence of the spreading in solar cells on admittance measurements could also be explained in terms of a simplified equivalent circuit [26] where C_W (figure 3) should be replaced by the circuit described in figure 12, where C_W^0 is the capacitance of the depletion region of the p–n junction placed under the contact grid. The photoactive area (which is not covered by the contact grid) is divided into k parts. C_W^n corresponds to the capacitance of the depletion region of the p–n junction of the nth part of the photoactive area and G_L^n is the lateral conductance of the nth part of the emitter layer and can be expressed as

$$G_L^n = qp\mu_p dl/x, \tag{4.1}$$

where p is the hole concentration in the p-emitter, μ_p is the hole mobility in the p-emitter, d is the emitter thickness, l is the digit length and x is the width of the part of the photoactive area.

Due to a relatively large ionization energy of Mg acceptors in GaInP (being equal to 39.7 meV for the doping level of 4×10^{17} according to [27]) the hole concentration depends on the temperature in the wide range as shown in figure 13, where p is calculated using Fermi–Dirac statistics. Assuming linear temperature dependence of the hole mobility (from 100 cm^2 s^{-1} V^{-1} at 100 K to 50 cm^2 s^{-1} V^{-1} at 300 K) and using geometrical parameters of the solar cell grid the equivalent capacitance of the circuit presented in figure 12 was calculated. The temperature behaviour of this capacitance normalized to the maximum value is presented in figure 13. The observed significant change in the capacitance with temperature will add to the capacitance step related to the interface potential barrier, and will lead to a significant error in the determination of this barrier height. Therefore, for reliable analysis admittance measurements should be performed on the structures with full coverage of top contacts only.

5. Conclusions

Admittance spectroscopy was shown to be sensitive to the band structure of III-phosphides interfaces. In particular, the possibility to determine the values of the effective potential barrier for majority carriers by direct measurement of the activation energy of a capacitance step was demonstrated. The obtained value of the effective potential barrier for holes at the p-AlInP/p-GaAs interface is found equal to 0.6 eV, which according to the simulations corresponds to the value of the valence band offset, and it is in good agreement with some previous results from the literature. The influence of the spreading resistance in p-GaInP emitter was shown to influence admittance measurements performed on solar cells, where the contact area is smaller than the emitter area. This can lead to significant errors in the determination of band offsets from the proposed method. Therefore, for further studies of other heterointerfaces such as p-GaInP/p-GaAs and n-AlInP/n-GaAs special mesa structures with full metal coverage of the top electrode should be fabricated.

Acknowledgments

This work was supported by the NATO Reintegration grant NR.RIG 982984 and by the Russian Foundation for Basic Research (RFBR), as well as by the CNRS in the framework of a joint Russian–French PICS project (no 4278 of CNRS, RFBR 07-08-92163).

References

[1] Kurtz S R, Olson J M, Friedman D J, Geisz J F, Bertness K A and Kibbler A E 1999 *Compound Semiconductor Surface Passivation and Novel Device Processing, Mater. Res. Soc. Symp. Proc.* vol 573, ed H Hasegawa *et al* (Warrendale, PA: Materials Research Society) p 95

[2] Gudovskikh A S, Kaluzhniy N A, Lantratov V M, Mintairov S A, Shvarts M Z and Andreev V M 2008 *Thin Solid Films* **516/20** 6739

[3] He X and Razeghi M 1993 *J. Appl. Phys.* **73** 3284

[4] Olson J M, Ahrenkiel R K, Dunlavy D J, Keyes B and Kibbler A E 1989 *Appl. Phys. Lett.* **55** 1208

[5] Dehaese O, Wallart X, Schuler O and Mollot F 1998 *J. Appl. Phys.* **84** 2127

[6] Liedenbaum C T H F *et al* 1990 *Appl. Phys. Lett.* **57** 2698

[7] Dawson M D and Duggan G 1993 *Phys. Rev.* B **47** 12598

[8] Dawson M D, Najda S P, Kean A H, Duggan G, Mowbray D J, Kowalski O P, Skolnick M S and Hopkinson M 1994 *Phys. Rev.* B **50** 11190

[9] Ishitani Y *et al* 1996 *J. Appl. Phys.* **80** 4592

[10] Vignaud D and Mollot F 2003 *J. Appl. Phys.* **93** 384

[11] Patel D, Hafich M J, Robinson G Y and Menoni C S 1993 *Phys. Rev.* B **48** 18031

[12] Watanabe M O and Ohba Y 1987 *Appl. Phys. Lett.* **50** 906

[13] Vurgaftman I, Meyer J R and Ram-Mohan L R 2001 *J. Appl. Phys.* **89** 5815

[14] Lang D V, Cohen J D and Harbinson J P 1982 *Phys. Rev.* B **25** 5285

[15] Gudovskikh A S, Kleider J P, Damon-Lacoste J, Roca i Cabarrocas P, Veschetti Y, Muller J-C, Ribeyron P-J and Rolland E 2006 *Thin Solid Films* **511–512** 385

[16] Lantratov V M, Kaluzhniy N A, Mintairov S A, Timoshina N K, Shvarts M Z and Andreev V M 2007 *Semiconductors* **41** 727

[17] Stangl R, Kriegel M and Schmidt M 2006 *Proc. 4th World Conf. on Photovoltaic Energy Conversion (Hawaii, USA)* vol 2, p 1350

[18] Sze S M 1981 *Physics of Semiconductor Devices* 2nd edn (New York: Wiley)

[19] Gomyo A, Suzuki T and Iijima S 1988 *Phys. Rev. Lett.* **60** 2645

[20] Bour D P, Shealy J R, Wicks G W and Schaff W J 1987 *Appl. Phys. Lett.* **50** 615

[21] Jiang C-S, Friedman D J, Moutinho H R and Al-Jassim M M 2006 *Proc. 4th World Conf. on Photovoltaic Energy Conversion (Hawaii, USA)* vol 1, p 853

[22] Adachi S 1985 *J. Appl. Phys.* **58** R1

[23] Anderson R L 1960 Germanium–gallium arsenide heterojunction *IBM J. Res. Dev.* **4** 283

[24] Zolper J C and Chui H C 1996 *Appl. Phys. Lett.* **68** 3473

[25] Kuo H C, Kuo J M, Wang Y C, Lin C H, Chen H and Stillman G E 1997 *J. Electron. Mater.* **26** 944

[26] Fahrner W R, Goesse R, Scherff M, Mueller T, Ferrara M and Neitzert H C 2005 *J. Electrochem. Soc.* **152** G819

[27] Chang C Y, Wu M C, Su Y K, Nee C Y and Cheng K Y 1985 *J. Appl. Phys.* **58** 3907